Available online at www.sciencedirect.com
ScienceDirect
Journal of the European Ceramic Society 30 (2010) 947–961
www.elsevier.com/locate/jeurceramsoc

Low temperature nanostructured zinc titanate by an aqueous particulate sol–gel route: Optimisation of heat treatment condition based on Zn:Ti molar ratio

M.R. Mohammadi [a,b,*], D.J. Fray [a]

[a] Department of Materials Science & Metallurgy, University of Cambridge Pembroke Street, Cambridge, CB2 3QZ, UK
[b] Department of Materials Science & Engineering, Sharif University of Technology Azadi Street, Tehran, Iran

Received 7 July 2009; received in revised form 16 September 2009; accepted 28 September 2009
Available online 28 October 2009

Abstract

Nanocrystalline zinc titanate ($ZnTiO_3$) thin films and powders with purity of 94% were produced at the low sintering temperature of 500 °C and the short sintering time of 1 h by a straightforward aqueous particulate sol–gel route. The effect of Zn:Ti molar ratio was studied on the crystallisation behaviour of zinc titanates. The prepared sols showed a narrow particle size distribution in the range 17–19 nm. X-ray diffraction (XRD) and Fourier transform infrared spectroscopy (FTIR) revealed that the powders contained mixtures of the rhombohedral-$ZnTiO_3$, cubic-ZnO, cubic-Zn_2TiO_4 phases, as well as the anatase-TiO_2 and the rutile-TiO_2 depending on the sintering temperature and Zn:Ti molar ratio. Moreover, it was found that Zn:Ti molar ratio and sintering temperature influence the preferable orientation growth of the zinc titanate, being on (2 1 1) planes for molar ratios of Zn:Ti = 25:75 and 50:50 and on (1 $\bar{1}$ 0) planes for molar ratio of Zn:Ti = 75:25 at sintering temperature of 600 °C. Transmission electron microscope (TEM) images showed that the average crystallite size of the powders annealed at 400 °C was around 2 nm and a gradual increase occurred up to 8 nm by heat treatment at 1000 °C. The activation energy for crystal growth of nanocrystalline $ZnTiO_3$ calculated in the range 07.86–14.79 kJ/mol. Field emission scanning electron microscope (FE-SEM) analysis revealed that the deposited thin films had mesoporous and nanocrystalline structure with the average grain size of 19–23 nm at 600 °C and 34–39 nm at 800 °C depending upon the Zn:Ti molar ratio.

Keywords: Zinc titanate; Aqueous particulate sol–gel; Nanostructure

1. Introduction

Titanium based ilmenite-type oxides with general formula $ATiO_3$ have been regarded as functional inorganic materials, because of their wide range applications in electrodes of solid oxide fuels (SOFCs),[1] metal–air barriers,[2] gas sensors,[3] and as high performance catalysts[4] for the complete oxidation of hydrocarbons or CO and NO_2 reduction. Zinc titanate ($ZnTiO_3$), being one member of this well-known family, may be used as paint pigment,[5] catalytic sorbent for the desulfurization of hot coal gases[6] and as gas sensor for the detection of NO, CO and, etc.[3] Recent studies have also found that it can be a useful candidate for microwave resonator materials and more importantly for low temperature co-fired ceramics.[7] The materials required to fabricate microwave devices should have a high dielectric constant ($\varepsilon_T > 20$), a low dissipation factor ($\tan(\delta) < 10^{-3}$), a small temperature coefficient of the resonant frequency (τ_f) and a small temperature coefficient of the dielectric constant (τ_ε).[8,9] Most of the known dielectrics, which have been employed for the present applications, have been usually synthesized by employing high temperature sintering, which is usually in the range 1200–1500 °C. In this regard, $ZnTiO_3$ is a potential candidate for microwave devices application because of the fact that it possess a high dielectric constant ($\varepsilon_T = 29$), a low dielectric loss ($\tan(\delta) < 10^{-3}$) and requires lower sintering temperature (~1100 °C).[10] However, the dielectric properties of $ZnTiO_3$ are sensitive to phase transitions and restrict its practical applications. It is, therefore, important to investigate the phase transition mechanism of zinc titanate materials with sintering temperature and Zn:Ti molar ratio.

* Corresponding author at: Department of Materials Science & Metallurgy, University of Cambridge Pembroke Street, Cambridge, CB2 3QZ, UK. Tel.: +44 79 5416 4928/+98 21 6616 5211.
E-mail addresses: mrm41@cam.ac.uk, mohammadi@sharif.edu (M.R. Mohammadi).

0955-2219/$ – see front matter © 2009 Elsevier Ltd. All rights reserved.
doi:10.1016/j.jeurceramsoc.2009.09.031

Based on the literature, three compounds are known to exist in the $ZnO–TiO_2$ system: Zn_2TiO_4 (zinc orthotitanate) with cubic spinel crystal structure, $Zn_2Ti_3O_8$ with cubic defect spinel structure and $ZnTiO_3$ (zinc metatitanate) with rhombohedral ilmenite structure.[11–13] Zn_2TiO_4 can easily be prepared by the conventional solid-state reaction of $2ZnO{\cdot}1TiO_2$ and is stable from room temperature to its liquid temperature (1418 °C). The metastable $Zn_2Ti_3O_8$ is regarded as a low-temperature form of $ZnTiO_3$ existing below 820 °C.[13] However, purely rhombohedral-$ZnTiO_3$ is not easily obtained because $ZnTiO_3$ decomposes into Zn_2TiO_4 and rutile-TiO_2 at temperature 945 °C.[11] It has been reported that the partial substitution of zinc with divalent cations (such as Co, Sr, Ba, Ni, and Mg) could enhance the stability of the rhombohedral phase as well as its microwave dielectric properties.[14] It should be noted that, the phase transitions of $ZnO–TiO_2$ system are relatively complex and sensitive to the starting materials, additives, and preparation method.

Zinc titanate is usually synthesized and crystallised by solid-state reaction at high temperatures.[11,15] Owing to limitations of solid-state synthesis, especially in terms of large $ZnTiO_3$ grain size and with uncontrolled and irregular morphologies and its contamination during repeated calcinations, several alternative chemical methods have been developed. Moreover, when a temperature below 1000 °C is used, an extended heat treatment is necessary for crystallisation.[16–18] This also results in crystal growth and therefore decreasing the desirable properties of the material. Chemical synthesis methods were also employed in order to reduce the crystallisation temperature. For example, K. Jothimurugesan and S.K. Gangwal[19] produced crystalline zinc titanate by co-precipitation method and subsequent heat treatment at 700 °C for 2 h. However, secondary phases were also observed in the product. S. Lew et al.[20] synthesized the same material by a citrate method and heat treatment at 720 °C for 12 h. As crystallisation only occurs after long sintering times, extensive grain growth also occurs. Amongst chemical routes, sol–gel techniques offer important advantages due to a low cost simple synthetic route, excellent compositional control, high homogeneity at the molecular level, feasibility of producing thin films on large and complex shapes and, the most significant one, low crystallisation temperature. Therefore, many efforts have been aimed to produce crystalline $ZnTiO_3$ with ilmenite structure at the low sintering temperature by sol–gel method. A.R. Phani and S. Santucci[21] prepared crystalline cubic-$ZnTiO_3$ thin film by a sol–gel method at 700 °C for 5 h, using titanium butoxide and zinc acetate dihydrate as starting materials, ethanol as solvent and ethylene glycol as additive. On further increasing the sintering temperature from 600 °C-5 h to 700 °C-5 h, apart from cubic-$ZnTiO_3$ phase, small amounts of rhombohedral phase of $ZnTiO_3$ was also observed. $ZnTiO_3$ powders were prepared by sol–gel method, including the Pechini process, using zinc acetate, titanium butoxide, ethanol, ethylene glycol and citric acid anhydrous by Y.S. Chang et al.[22] They obtained crystalline $ZnTiO_3$ as well as some traces of Zn_2TiO_4 and rutile-TiO_2 phases after sintering at 800 °C for 6 h. These authors reported zinc titanate ($ZnTiO_3$) powders of the perovskite structure by conventional solid-state reaction, using pure ZnO and TiO_2 powders as the starting materials.[23] Mixtures of crystalline $ZnTiO_3$, Zn_2TiO_4 and rutile-TiO_2 phases were achieved at 800 °C for 12 h. Zinc titanate powders were also prepared by sol–gel processing, using zinc acetate dihydrate and titanium butoxide as precursors by L. Zhao et al.[24] A small amount of amorphous $ZnTiO_3$ phase, as well as Zn_2TiO_4 and rutile-TiO_2, was detected in the powders sintered at 700 °C for 2 h. Crystalline phases of $ZnTiO_3$, Zn_2TiO_4 and rutile-TiO_2 with sharp X-ray diffraction peaks were obtained after sintering at higher temperatures of 900 °C for 2 h. L. Hou et al.[25] reported hexagonal $ZnTiO_3$ powders by sol–gel processing with zinc nitrate hexahydrate and titanium butoxide materials. Although they reported that a pure hexagonal $ZnTiO_3$ was obtained at 800 °C, some trace of rutile-TiO_2 and Zn_2TiO_4 were seen in the XRD pattern. The sintering time was not reported in their work. A.R. Phani et al.[26] prepared nanocrystalline $ZnTiO_3$ films by a sol–gel route, using titanium butoxide and zinc acetate as precursors, 2-methoxy ethanol as solvent, acetyl-acetone as a complexing and chelating agent and cetyltrimethyl ammonium bromide as surfactant. They studied the effect of conventional annealing and microwave irradiation on crystallisation process. In case of conventional annealing, the films sintered at 400 °C exhibited amorphous nature and films sintered at 800 °C for 3 h showed sharp, high intensity peaks, corresponding to cubic phase of $ZnTiO_3$ as well as some traces of rutile-TiO_2 and Zn_2TiO_4 phases located at $2\theta = 27.4°$ and $2\theta = 42.7°$ reflections, respectively. Broad and low intensity peaks with preferential growth of (3 1 1) cubic phase of $ZnTiO_3$ was observed for the films after exposure to microwave heating at 900 W for 10 min. Y.L. Chai et al.[27] synthesized nano-sized $ZnTiO_3$ powders by the Pechini process, using zinc acetate, ethylene glycol, titanium butoxide, citric acid anhydrous. The powder was a mixture of $ZnTiO_3$ and Zn_2TiO_4 in the range 700–1000 °C. The optimum temperature for the crystallisation of $ZnTiO_3$ was reported at 800 °C for 6 h and some traces of Zn_2TiO_4 and rutile-TiO_2 were also observed. S.K. Manik and S.K. Pradhan[28] produced nanocrystalline $ZnTiO_3$ and Zn_2TiO_4 phases by high-energy ball milling. They observed that after 3 h of milling, peak positions of both the $ZnTiO_3$ and Zn_2TiO_4 phases become prominent. Mixtures of $ZnTiO_3$, Zn_2TiO_4 and a small amount of rutile-TiO_2 were obtained after 6 h of milling. Consequently, the optimum crystallisation condition of preparing crystalline zinc titanate by polymeric sol–gel methods was obtained at 700 °C for 5 h or at 900 °C for 2 h in the previous studies.

The aim of the present work is to develop a strategy for lowering the sintering temperature and time for crystallisation of nanostructured zinc titanate material by employing a suitable aqueous particulate sol–gel route rather than the polymeric sol–gel methods reported previously. This process can be defined as an environmentally friendly processing as it uses an aqueous solution. One of the advantages of the present method is using an alternative to acetate (i.e., zinc chloride) as a zinc source to produce crack-free thin films. Since the pores in particulate sol–gel processes are much larger than that found in polymeric sol–gel route, the capillary stress and therefore the shrinkage decrease during heat treatment. Besides controlling the phase structure, composition homogeneity, crystallite size

Table 1
$ZnTiO_3$ sols prepared with various molar ratios.

Sample reference	Zn:Ti (mol%/mol%)	HPC (g/100 ml)
ZT13	25:75	1.5
ZT11	50:50	1.5
ZT31	75:25	1.5

and monodispersity and microstructure, the cost of the product is an important concern in developing technologies for synthesis of zinc titanate. Therefore, starting with a low cost precursor such as zinc chloride rather than zinc acetate may reduce the total cost of production. Thus, the present method is a simple and cheap process with capability of producing zinc titanate thin films and powders with faster production rate in comparison to the previous polymeric sol–gel methods reported in the literature. Furthermore, the effect of Zn:Ti molar ratio, as the sol–gel processing parameter, is studied on crystallisation behaviour of zinc titanates. Consequently in this paper we report, for the first time, zinc titanate material with mesoporous and nanocrystalline structure after sintering at the low temperature of 500 °C. The effect of Zn:Ti molar ratio and sintering temperature on physical and chemical characteristics of the prepared thin films and powders is also discussed.

2. Experimental

2.1. Preparation of the $ZnTiO_3$ sols

Titanium tetraisopropoxide (TTIP) with a normal purity of 97% (Aldrich, UK), and zinc chloride ($ZnCl_2$) with a normal purity of 98% (Fluka, UK) were used as titanium and zinc precursors, respectively. Analytical grade hydrochloric acid (HCl) 37% (Fisher, UK) was used as a catalyst for the peptisation and deionised water was used as a dispersing media. Hydroxypropyl cellulose (HPC) with an average molecular weight of 100,000 g mol^{-1} (Acros, USA) was used as a polymeric fugitive agent (PFA).

The $ZnTiO_3$ systems were prepared by an aqueous particulate sol–gel method. The first step was the preparation of titanium dioxide sol based on our previous study.[29] The molar ratio of TTIP:HCl:H_2O was 1.0:0.5:351.3, which makes a 0.15 M TiO_2 sol. The water–acid mixture was stabilized at 70 °C, and this temperature was kept constant throughout the experiment, together with continuous stirring. TTIP was added, forming a white thick precipitate, which gradually peptized after 2 h to form a clear sol. The clear sol was cooled to room temperature. In different beakers, predetermined amounts of $ZnCl_2$ and HPC were dissolved in deionised water at room temperature and stirred for 30 min to obtain the desirable Zn:Ti molar ratios, as shown in Table 1. HPC concentration was defined according to the previous study,[30] which induced the highest surface area. This solution was then mixed with TiO_2 sol, stirring during 2 h.

All sols were stable and no gelation occurred during preparation. Sols were characterised in particle size by dynamic light scattering technique (DLS) using a Malvern ZetaSizer 3000HS at 20 °C using a 10 mW He-Ne laser, 633 nm wavelength and 90° fixed scattering angle. The stability of prepared precursors was also determined with Zeta potential using the same instrument.

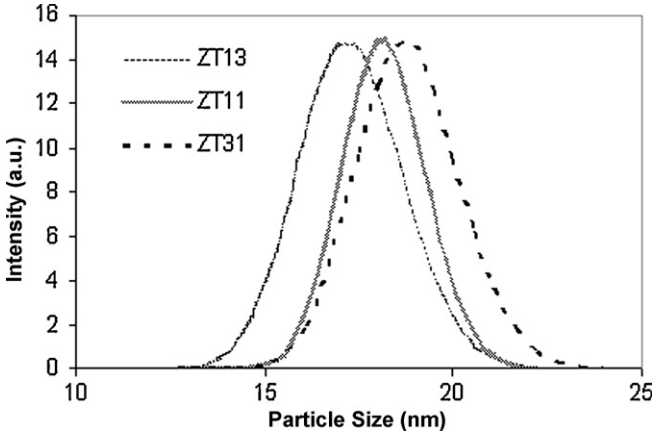

Fig. 1. Particle size distributions of prepared sols.

2.2. Preparation of $ZnTiO_3$ thin films

Films were deposited onto 10 mm × 5 mm × 1 mm quartz substrates, in order to avoid TiO_2 peak overlapping with the peaks of the most commonly used Si and Al substrates. Before deposition, substrates were cleaned using a high power sonic probe consecutively in water, ethanol and acetone, and dried at 70 °C for 15 min. One layer of film was deposited by dip-coating. The substrates were immersed in the precursor and kept there for a few minutes, followed by a withdrawing speed of 0.6 cm min^{-1}. The subsequent heat treatment was optimised as follows. The films were dried at 150 °C for 1 h, annealed at a rate of 5 °C min^{-1} up to different temperatures (400, 600, 800 and 1000 °C) and held at these temperatures for 1 h in air. Films were characterised in microstructure using a scanning electron microscope FE-SEM JEOL 6340 and in topography using atomic force microscope AFM Nanoscope III, Digital Instrument Inc. The average grain size of the films was determined based on FE-SEM and AFM micrographs.

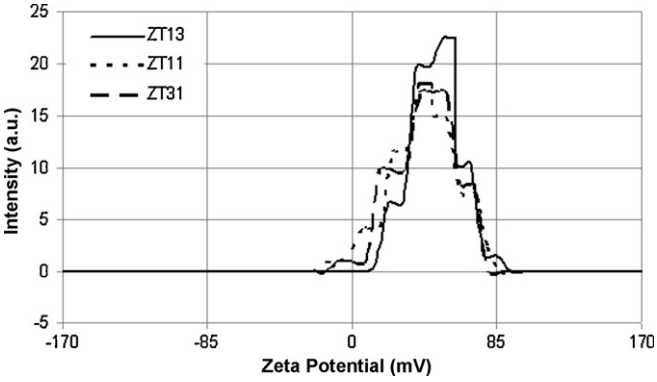

Fig. 2. Zeta potential of the particles in prepared sols (pH 1–2).

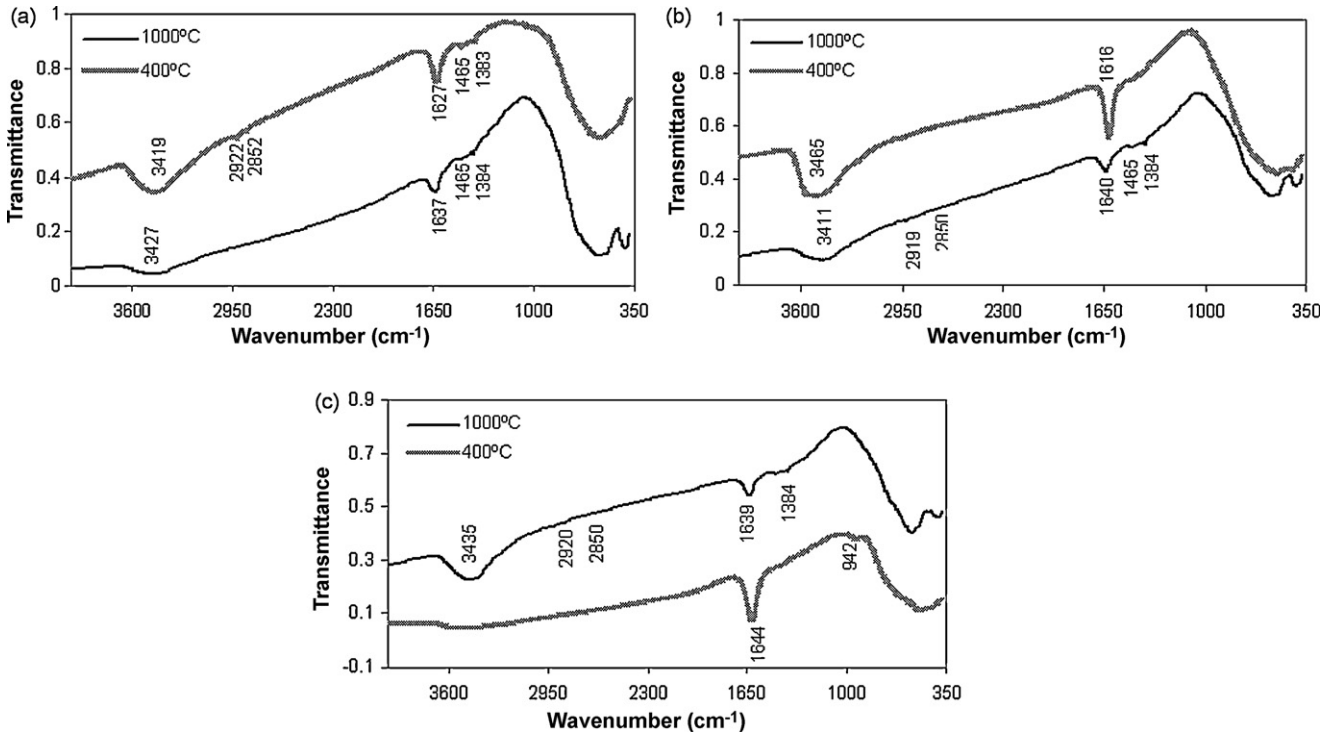

Fig. 3. FTIR spectra of $ZnTiO_3$ powders sintered at 400 and 1000 °C: (a) ZT13, (b) ZT11 and (c) ZT31.

2.3. Synthesis of $ZnTiO_3$ powders

Powders were prepared by drying each sol at room temperature for 72 h. Powders were thermally processed in the same way as the films. These powders were characterised in the phase composition and crystallite size using an X-ray diffraction diffractometer (XRD) Philips E'pert PW3020, Cu-K_α and transmission electron microscope (TEM) JEOL 200CX. The crystallite size of phases, including rhombohedral-$ZnTiO_3$, cubic-$ZnTiO_3$, cubic-Zn_2TiO_4, hexagonal-ZnO, anatase-TiO_2 and rutile-TiO_2, which matched with database in JCPDS cards number of 85-0547, 39-0190, 77-0014, 80-0075, 84-1286 and 86-0147, was calculated from their reflections using the Debye-Scherrer equation[31]:

$$d = \frac{k\lambda}{B\cos\theta} \tag{1}$$

where d is the crystallite size, k a constant of 0.9, λ the X-ray wavelength of Cu which is 1.5406 Å, θ the Bragg angle in degrees, and B the full width at half maximum (FWHM) of the peak. The $ZnTiO_3$ and TiO_2 contents of the powders were estimated by the following equations:

$$X_{ZT} = \frac{\sum_{i=1}^{N} I_{ZT_i}}{\sum_{i=1}^{N} I_{ZT_i} + \sum_{j=1}^{N} I_{S_j}} \tag{2}$$

$$X_T = \frac{\sum_{i=1}^{N} I_{T_i}}{\sum_{i=1}^{N} I_{T_i} + \sum_{j=1}^{N} I_{S_j}} \tag{3}$$

where X_{ZT} and X_T are the contents of zinc titanate and titania, respectively, I_{ZT_i} and I_{T_i} are the intensity of the zinc titanate and titania reflections, respectively and I_{S_j} is the reflection intensity for the rest of phases. The activation energy for crystal growth of $ZnTiO_3$ can be calculated by Arrhenius equation reported by Bolen et al.[32]:

$$\log(d) = -\frac{Q}{2.303RT} + C \tag{4}$$

where d is the average crystallite size of $ZnTiO_3$, Q is activation energy, T is absolute temperature, R is ideal gas constant and C is intercept.

Powders were also characterised in thermal behaviour using simultaneous differential thermal analysis TA-SDTQ600, with a heating rate of 5 °C min^{-1} in air up to 1000 °C and bond configuration by Fourier transform infrared spectroscopy (FTIR) using a Bruker Optics Tensor 27 analyser in the region 4000–350 cm^{-1}.

3. Results and discussion

3.1. Particle sizes and charges

Fig. 1 shows the mean size of the particles for prepared sols. It can be observed that all sols had a narrow particle size distribution, being 17.0, 18.2 and 19.1 nm for ZT13, ZT11 and ZT31 sols, respectively. The particle size of the TiO_2 sol reported in our previous study was 17.0 nm.[33] Therefore, no significant increase in the mean size of the particles was observed for $ZnTiO_3$ sols, which confirms that stability of sols is maintained when a solution of zinc chloride is added into TiO_2 sol. To investigate how the hydrodynamic diameter of the particles is affected by ionic strength of the medium various HCl/(Ti + Zn) molar ratios, with equal HCl concentrations, were used for different sols. The higher HCl/(Ti + Zn) molar ratio, the higher the surface

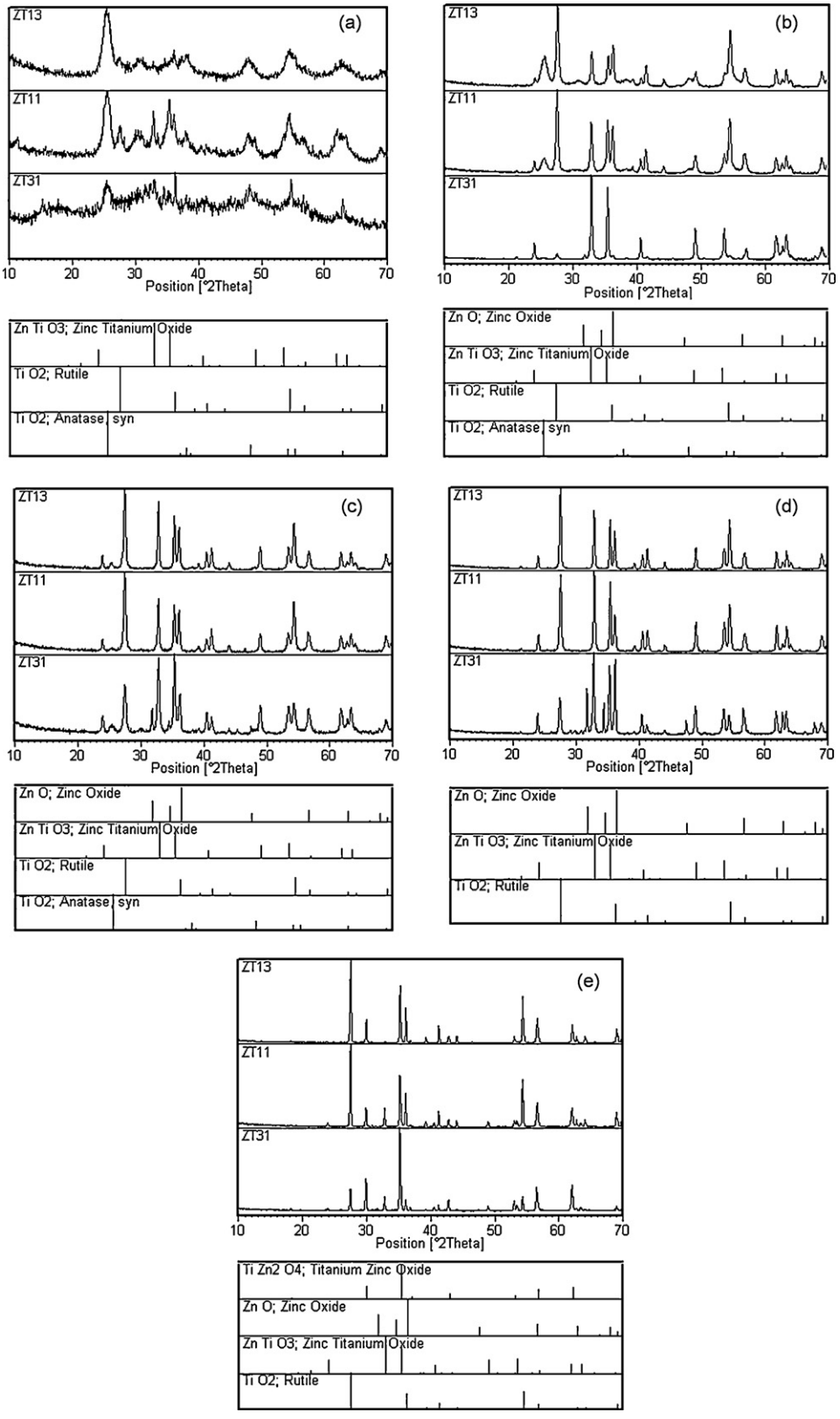

Fig. 4. XRD patterns of ZT13, ZT11 and ZT31 powders sintered at (a) 400 °C, (b) 500 °C, (c) 600 °C, (d) 800 °C and (e) 1000 °C for 1 h.

charge around the particles, resulting in the prevention coagulation and flocculation of particles by electrostatic repulsion. Consequently, ZT13 sol had the smallest particle size amongst all sols.

The zeta potential of the particles is shown in Fig. 2. The stability of the sols was achieved by both electrostatic stabilisation and steric mechanisms. The electrostatic stabilisation mechanism within the sol has an effect on particle interaction due to

Table 2
Distribution of phases for prepared powders determined by X-ray diffraction.

	400 °C	500 °C	600 °C	800 °C	1000 °C
ZT13	ZT + A + R	ZT + A + R	ZT + A + R	ZT + R	ZT + Z_2T + R
ZT11	ZT + A + R	ZT + A + R	ZT + A + R	ZT + R	ZT + Z_2T + R
ZT31	ZT + A + R	ZT + ZO + A + R	ZT + ZO + A + R	ZT + ZO + R	ZT + Z_2T + ZO + R

A: anatase-TiO_2; R: rutile-TiO_2; ZT: rhombohedral-$ZnTiO_3$; ZO: hexagonal-ZnO; Z_2T: cubic-Zn_2TiO_4.

the distribution of charged species, whereas the steric repulsion mechanism involves PFA added to the system adsorbing onto the particle surface and preventing the particle surfaces from coming into close contact. It has been reported that generally speaking the range of zeta potential in unstable sols goes from −30 to +30 mV.[34] The average zeta potential of particles in ZT13, ZT11 and ZT31 sols was 47.1, 40.6 and 38.2 mV, respectively. As mentioned earlier, the surface charge around the particles of ZT13 sol is higher than that of for the other sols, resulting in higher zeta potential value for this sol. All sols were found to be stable over 5 months since their zeta potential was constant during this period.

3.2. Infrared characteristics

The bond configuration of $ZnTiO_3$ powders sintered at 400 and 1000 °C for 1 h is shown in Fig. 3. It is known that the absorption bands in the range 1100–1000 cm^{-1} are attributed to the OR groups linked to Ti such as OC_3H_7, OC_4H_7 and OC_2H_5.[35] The characteristic absorption peak of (OR) group of titanium isopropoxide, which was the precursor of the sols, is in range 1085–1050 cm^{-1}.[36] Owing to the fact that no absorption peak was detected in this range for both annealing temperature, it is concluded that all four (OR) groups of titanium isopropoxide were substituted with (OH) groups of water. Thus, a full conversion of TTIP is obtained by the hydrolysis reaction, resulting in formation of TiO_2 particles. The band due to the Ti–O stretching vibration is found in the range 700–400 cm^{-1}.[37] Therefore, the set of three bands at 606 cm^{-1} for ZT13, 541 cm^{-1} for ZT11 and 536 cm^{-1} for ZT31 powders sintered at 1000 °C are considered to be the above stretching vibrations, corresponding to the presence of TiO_6 group existing in all forms of $ZnTiO_3$ and Zn_2TiO_4. It is worth to note that the wavenumber for absorption bands of Ti–O octahedra decreased with increasing Zn:Ti molar ratio. Two weak bands at 1383 cm^{-1} and in the range 1465–1445 cm^{-1} are due to the stretching vibration of $\delta(CH_2–CH_3)$ and C–O–H, respectively for the powders sintered at 400 °C. Moreover, the bands at 2922 and 2852 cm^{-1} are due to the stretching vibration of the C–H bond of organic compounds. These can be related to the employment of HPC as a PFA. It can be observed that most organic species in the precursor powders disappeared after sintering at 1000 °C, which agrees with the XRD analysis (see Section 3.3.1). Water incorporation is found with the peak in the range 1650–1627 cm^{-1} for the powders sintered at both temperatures. The intensity if this peak was reduced with increasing sintering temperature up to 1000 °C. It is known that the broad band in the range 3220–3097 cm^{-1} is due to the stretching vibration of the hydroxyl (O–H) bond.[36] The results are in good agreement with those reported by Y.L. Chai et al.[27] and L. Hou et al.[25]

3.3. Crystal characterisation

3.3.1. XRD analysis

Fig. 4 shows the X-ray diffraction patterns of the powders sintered in the range 400–1000 °C for 1 h. In addition, the distribution of phases determined by XRD is summarized in Table 2. The anatase-TiO_2 and the rutile-TiO_2 have tetragonal structure, zinc titanate ($ZnTiO_3$) has rhombohedral and cubic structures, titanium zinc oxide (Zn_2TiO_4) show face-centered cubic structure and zinc oxide (ZnO) possesses hexagonal structure. The powders sintered at 400 °C showed poor crystalline structure containing mixtures of anatase-TiO_2, rutile-TiO_2, and rhombohedral-zinc titanate ($ZnTiO_3$) phases. The rutile phase was determined by a peak at $2\theta = 27.4°$ (1 1 0) and $2\theta = 36.0°$ (1 0 1) for ZT13 and ZT31 powders, respectively, whereas both peaks were observed for ZT11 powder. It can be observed that the crystalline phases including anatase-TiO_2, rutile-TiO_2, zinc oxide, zinc titanate and titanium zinc oxide were formed after sintering at 500 °C and higher temperatures. Therefore, crystalline zinc titanate with rhombohedral structure was produced at the low temperature of 500 °C for 1 h. The anatase phase was detected by a peak at $2\theta = 25.3°$ (1 0 1) for all powders annealed at 500–600 °C. This phase was stable up to 600 °C and transformed to rutile phase at $T \geq 800$ °C. Therefore, the anatase to rutile phase transformation temperature was mea-

Table 3
Influence of the Zn:Ti molar ratio on preferable orientation growth of the phases.

		Zn:Ti = 25:75	Zn:Ti = 50:50	Zn:Ti = 75:25
$ZnTiO_3$	500 °C	(2 1 1)	(2 1 1)	(1 $\bar{1}$ 0)
	600 °C	(2 1 1)	(2 1 1)	(1 $\bar{1}$ 0)
	800 °C	(2 1 1)	(2 1 1)	(2 1 1)
	1000 °C	(1 $\bar{1}$ 0)	(1 $\bar{1}$ 0)	(1 $\bar{1}$ 0)
Rutile-TiO_2 (600–1000 °C)		(1 1 0)	(1 1 0)	(1 1 0)
Zn_2TiO_4 (600–1000 °C)		(2 2 0)	(2 2 0)	(2 2 0)

Table 4
Influence of the annealing temperature on preferable orientation growth of the phases for all Zn:Ti molar ratios.

	500 °C	600 °C	800 °C	1000 °C
$ZnTiO_3$	(2 1 1)	(2 1 1)	(2 1 1)	(11$\bar{0}$)
Rutile-TiO_2	(1 1 0)	(1 1 0)	(1 1 0)	(1 1 0)
ZnO	(1 0 1)	(1 0 1)	(1 0 1)	(1 1 0)

sured at 800 °C. Zinc oxide was only detected for ZT31 powder at $T \geq 500$ °C. This phase was detected by three small peaks at $2\theta = 31.7°$ (1 0 0), $2\theta = 34.4°$ (0 0 2) and $2\theta = 47.5°$ (1 0 2). In addition, Zn_2TiO_4 phase was formed for all Zn:Ti molar ratios at high temperature of 1000 °C. Three peaks were related to this phase, being at $2\theta = 62.1°$ (4 4 0), $2\theta = 42.7°$ (4 0 0) and $2\theta = 18.2°$ (1 1 1), in a sequence of their intensities. Consequently, it can be concluded that the phase composition of the powders depends on the Zn:Ti molar ratio as well as the sintering temperature.

It is worth to note that the preferable orientation growth of the phases depends on the Zn:Ti molar ratio and sintering temperature. For all sintering temperatures, by increasing the Zn:Ti molar ratio to 75:25 the intensity of the rutile-TiO_2 at $2\theta = 27.4°$ (1 1 0) and $2\theta = 54.3°$ (2 1 1) reflections were reduced, while the intensity of rhombohedral-$ZnTiO_3$ at $2\theta = 35.3°$ (1 $\bar{1}$ 0), $2\theta = 48.9°$ (2 2 0) and $2\theta = 63.4°$ (1 $\bar{2}$ 1) reflections were increased. Moreover, cubic-$ZnTiO_3$ phase, matched with database in JCPDS card number of 39-0190, was detected at $2\theta = 31.9°$ (3 0 0) for Zn:Ti = 75:25 (molar ratio) at 600 and 800 °C. The influence of the Zn:Ti molar ratio on preferable orientation growth of each phase is summarized in Table 3. At sintering temperatures of 800 and 1000 °C, preferable orientation growth of rhombohedral-$ZnTiO_3$ was independent on Zn:Ti molar ratio, being on (1 $\bar{1}$ 0) planes at $2\theta = 35.3°$ and on (2 1 1) planes at $2\theta = 32.8°$, respectively. At sintering temperature of 500–600 °C, the preferable orientation growth of this phase depends on Zn:Ti molar ratio, being on (1 $\bar{1}$ 0) planes at $2\theta = 35.3°$ for the zinc dominant powders (Zn:Ti $\geq$ 75:25 molar ratio) and on (2 1 1) planes at $2\theta = 32.8°$ for rest of the powders (i.e., Zn:Ti < 75:25 molar ratio). Furthermore, the preferable orientation growth of the rutile-TiO_2 and Zn_2TiO_4 were independent on Zn:Ti molar ratio, being on (1 1 0) planes at $2\theta = 27.4°$ and (2 2 0) planes at $2\theta = 29.9°$, respectively.

For ZT13 powder (Zn:Ti = 25:75 molar ratio), the intensity of rhombohedral-$ZnTiO_3$ at $2\theta = 32.8°$ (2 1 1), $2\theta = 40.5°$

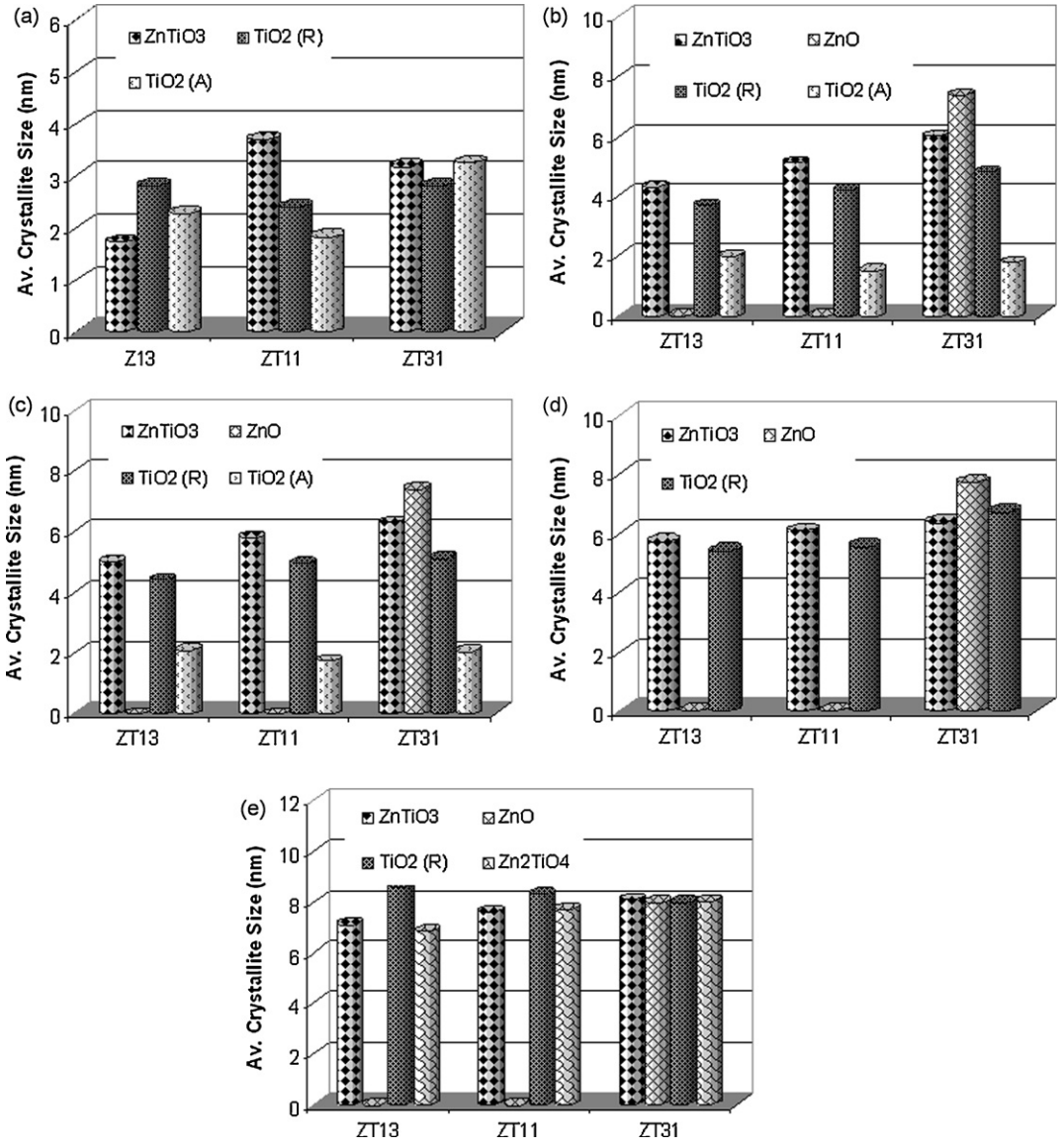

Fig. 5. Effect of Zn:Ti molar ratio on crystallite size of various phases for the powders sintered for 1 h at (a) 400 °C, (b) 600 °C, (c) 800 °C and (d) 1000 °C.

(2 1 0) and $2\theta = 53.4^\circ$ (3 2 1) reflections was reduced and the two peaks at $2\theta = 48.9^\circ$ (2 2 0) and $2\theta = 63.4^\circ$ (1 $\bar{2}$ 1) reflections were diminished by increasing sintering temperature up to 1000 °C. For ZT11 and ZT31 powders, the intensity of rhombohedral-$ZnTiO_3$ at $2\theta = 23.9^\circ$ (1 1 0) and at $2\theta = 41.5^\circ$ (1 1 $\bar{1}$) reflections, besides the above mentioned reflections, for ZT13 powder, were decreased by increasing sintering temperature up to 1000 °C. In addition, by increasing the sintering temperature the intensity of the rutile-TiO_2 at $2\theta = 27.4^\circ$ (1 1 0), $2\theta = 36.1^\circ$ (1 0 1) and $2\theta = 54.3^\circ$ (2 1 1) reflections were also decreased for ZT11 and ZT31 powders. The maximum intensity of ZnO phase at $2\theta = 31.7^\circ$ (1 1 0), $2\theta = 34.4^\circ$ (0 0 2) and $2\theta = 67.9^\circ$ (1 1 2) reflections were detected at sintering temperature of 800 °C. The influence of the sintering temperature on preferable orientation growth the phases is summarized in Table 4. For rhombohedral-$ZnTiO_3$, the preferable orientation growth was on (2 1 1) planes at $2\theta = 32.8^\circ$ and on (1 1 $\bar{0}$) planes at $2\theta = 35.3^\circ$ at 500–800 and 1000 °C, respectively. For ZnO, it was on (1 0 1) planes at $2\theta = 36.2^\circ$ and (1 1 0) planes at $2\theta = 56.5^\circ$ at 500–800 and 1000 °C, respectively. The preferable orientation growth of rutile-TiO_2 was independent on the sintering temperature, being on (1 1 0) planes at $2\theta = 27.4^\circ$.

Consequently in comparison to the conventional ceramics processes[11] and the previous sol–gel methods mentioned in the Introduction, crystalline zinc titanate ($ZnTiO_3$) powder with rhombohedral structure was successfully produced at the low temperature of 500 °C and the short sintering time of 1 h by a simple particulate sol–gel process aided by zinc chloride as a zinc source. This can be related to the very short-range diffusion path of the elements during heat treatment due to ultra fine crystallite size. Furthermore, this method has a potential for producing mixture of multi oxides by controlling the process parameters, i.e., the Zn:Ti molar ratio and sintering temperature. For example, mixtures of various oxides such as ZT + A + R, ZT + ZO + A + R, ZT + R, ZT + ZO + R, ZT + Z_2T + R and ZT + Z_2T + ZO + R were produced by the present method.

The effect of Zn:Ti molar ratio on crystallite size of the powders sintered in the range 400–1000 °C for 1 h is shown in Fig. 5. The average crystallite size of the powders sintered at 400 °C was in the range 2.3–3.0 nm and a gradual increase occurred up to 8 nm after heat treatment at 1000 °C. Therefore,

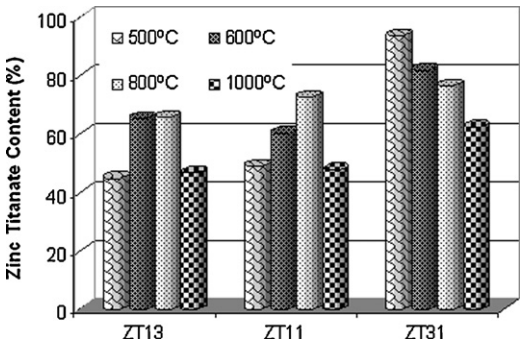

Fig. 6. Effect of Zn:Ti molar ratio and sintering temperature on $ZnTiO_3$ percentage.

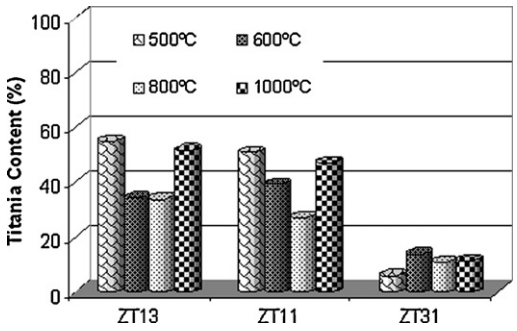

Fig. 7. Effect of Zn:Ti molar ratio and sintering temperature on titania percentage (in the forms of anatase and rutile phases).

the applied sol–gel process is an effective method for production of zinc titanate powders with high thermal stability against sintering at elevated temperatures. It is evident that the crystallite size of $ZnTiO_3$ phase increased with increasing Zn:Ti molar ratio for the powders sintered at 400–1000 °C. Moreover, for the powders sintered at 1000 °C the crystallite size of Zn_2TiO_4 phase increased with increasing Zn:Ti molar ratio, whilst the reverse trend was obtained for the crystallite size of rutile-TiO_2. On the other hand, the crystallite sizes of rutile-TiO_2 increased with increasing Zn:Ti molar ratio in the temperature range 500–800 °C. Finally, the smallest average crystallite size was achieved for the titanium dominant powder (i.e., ZT13 powder) at all sintering temperatures 400–1000 °C.

Fig. 6 shows $ZnTiO_3$ content based on the Zn:Ti molar ratio and sintering temperature. Firstly, the effect of sintering temperature at constant Zn:Ti molar ratio is explained: The zinc titanate content of ZT13 and ZT11 powders first increased and then decreased with increasing the sintering temperature. Therefore, the maximum $ZnTiO_3$ percentages of 66% and 73% were obtained for ZT13 and ZT11 powders annealed at 800 °C, respectively. This can be explained by the fact that the crystallisation process improves with increasing the sintering temperature. But there is a limit to this behaviour, as heat treatment at high temperature results in decomposition of $ZnTiO_3$ into Zn_2TiO_4 and rutile-TiO_2 phases. This phenomenon is also previously reported at high temperature of 945 °C.[27,22] The maximum $ZnTiO_3$ percentage of 94% was achieved for ZT31 powder after sintering at 500 °C. Therefore, if one accepts the above mentioned explanation for the reduction of $ZnTiO_3$ content

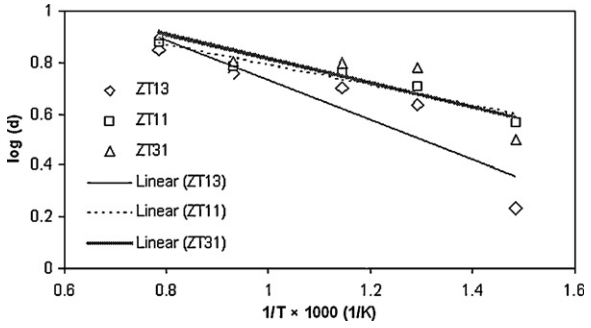

Fig. 8. A plot of log(d) versus the reciprocal of absolute temperature ($1/T$) × 1000 to determine the activation energy of $ZnTiO_3$ crystallite growth (◇: ZT13, □: ZT11 and △: ZT31).

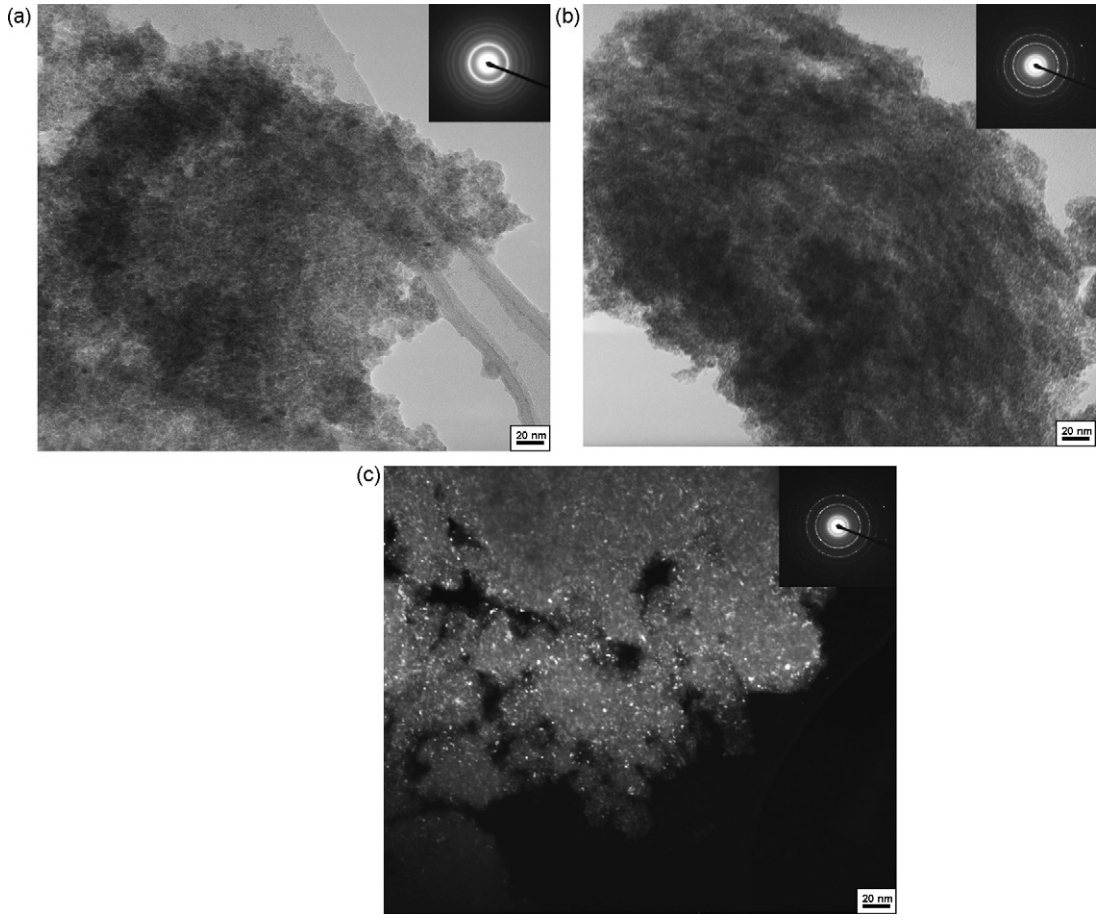

Fig. 9. TEM analysis: bright or dark filed plane-view images of ZT11 powders sintered at: (a) 400 °C, (b) 600 °C and (c) 1000 °C.

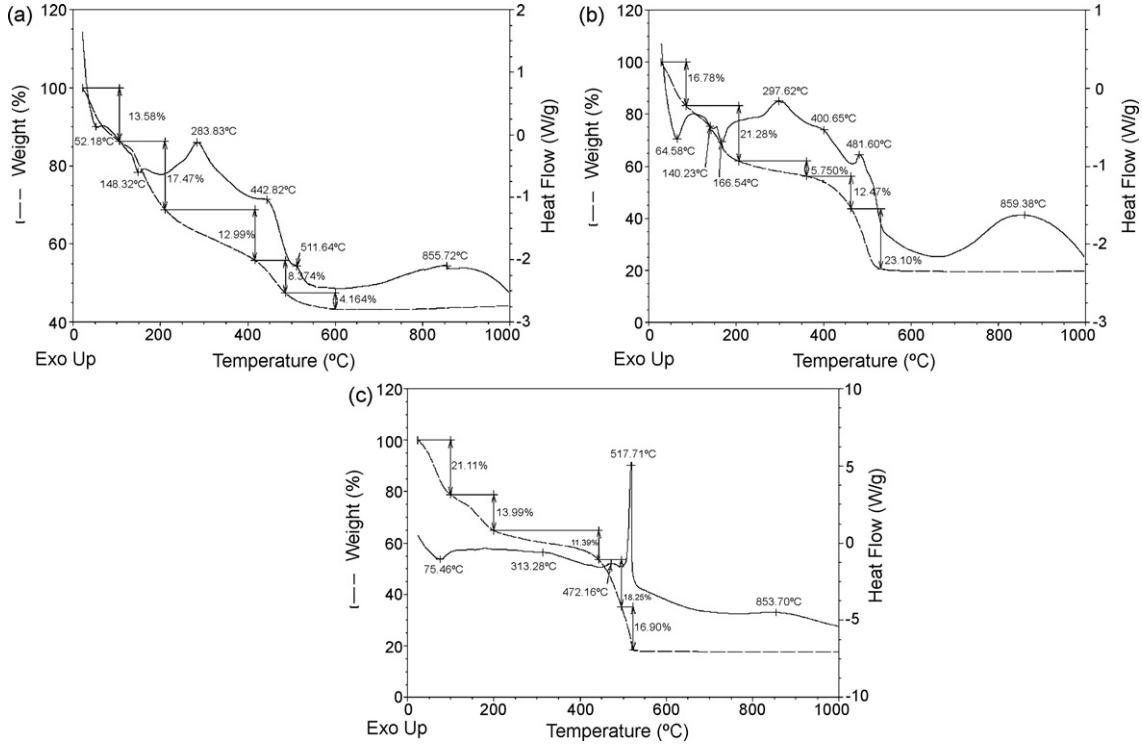

Fig. 10. SDT curves of (a) ZT13, (b) ZT11 and (c) ZT31 powders dried at room temperature for 72 h. The scan rate was 5 °C min^{-1}, performed in air.

with increasing the sintering temperature, it can be concluded that the decomposition temperature of $ZnTiO_3$ decreased down to 600 °C with increasing Zn:Ti molar ratio ≥75:25. This is an acceptable explanation, since the driving force of $ZnTiO_3$ decomposition is provided by increasing zinc concentration rather than increasing the sintering temperature.

Secondly, the effect of Zn:Ti molar ratio at constant sintering temperature can be explained: it can be seen that, zinc titanate content increased with increasing Zn:Ti molar ratio for all sintering temperatures. This can be related to decreasing the non-reacted TiO_2 content with zinc precursor. This was also confirmed by calculating the amount of anatase and rutile phases at various Zn:Ti molar ratios and sintering temperatures, as shown in Fig. 7.

The $ZnTiO_3$ powders with average particle size in the range 20–50 nm sintered at 600–900 °C were reported by Y.L. Chai et al.[27] A.R. Phani et al.[26] prepared sol–gel derived $ZnTiO_3$ thin films with crystallite size in the range 43–57 and 6.5–10.5 nm by heat treatment of conventional annealing at 400–800 °C and microwave annealing at 300–900 W, respectively. The average particle sizes in the range 7.7–9.0 nm for $ZnTiO_3$, 6.3–9.1 nm for Zn_2TiO_4, 2.9–8.6 nm for ZnO and 24.2–86.2 nm for rutile-TiO_2 were obtained for powders prepared by S.K. Manika, S.K. Pradhan[28] using high-energy ball milling with milling times of 1–6 h. Y.S. Chang et al.[23] produced powders of $ZnTiO_3$ by conventional solid-state reaction with the average crystallite size in the range 540–900 nm in the temperature region of 700–900 °C. They also reported $ZnTiO_3$ powders with the average crystalline size of 18–31 nm by a sol–gel technique including the Pechini process.[22] Therefore, in the present work, not only the rhombohedral-$ZnTiO_3$ powder with purity of 82% was synthesized at the low temperature of 600 °C and short sintering time of 1 h, but also one of the smallest crystallite size reported in the literature was obtained.

Fig. 8 illustrates a plot of logarithm of $ZnTiO_3$ crystallite size versus the reciprocal of absolute temperature. Based on the slope of the lines, the activation energies of $ZnTiO_3$ crystallite growth for ZT13, ZT11 and ZT31 powders were calculated as 14.79, 07.86 and 09.07 kJ/mol, respectively. Therefore, ZT11 powder had the lowest activation energy for crystal growth of $ZnTiO_3$. In addition, the calculated activation energies of the powders are lower than that of the bulk material (i.e., 315.5 kJ/mol[38]). This is expected because the nano-sized grains have a higher surface area to volume ratios compared to bulk, which increase the total surface energy. Thus, less energy is required to induce the crystal growth. Y.S. Chang et al.[23] calculated the activation energy for crystallite growth of $ZnTiO_3$, prepared by conventional solid-state reaction using metal oxides, about 48.84 kJ/mol. Furthermore, they[22] reported the activation energy for crystallite growth of nano-sized $ZnTiO_3$, synthesized by a sol–gel technique including the Pechini process, around 20.83 kJ/mol.

3.3.2. TEM analysis

The TEM analysis is better than XRD technique for measuring the average crystallite size, since it is direct and less likely to be affected by experimental errors and/or other properties of the particles such as internal strain or distribution in the size of the lattice parameter. Thus, Fig. 9 highlights TEM bright or dark field images of ZT11 powders sintered at 400–1000 °C. As can be seen, all powders exhibited uniform morphology in particle size with spherical shape. Furthermore, the relative electron diffraction pattern indicates a random orientation for the powders. The insets show ill defined rings arising from poor crystallite structure for the powders sintered at 400 °C, whereas well defined rings are observed for those sintered in the range 600–1000 °C, resulting in crystalline structure. The average crystallite sizes of the powders are around 2 and 8 nm at 400 and 1000 °C, respectively, which are consistent with those obtained by XRD analysis. Y.L. Chai et al.[27] measured a crystallite size of 30 nm for $ZnTiO_3$ powders sintered at 800 °C for 6 h by TEM analysis.

3.4. Thermal analysis

Simultaneous differential thermal analysis (SDT) of the powders is shown in Fig. 10. In addition, the description of peak position and weight loss of the powders determined by this analysis is summarized in Table 5. All powders undergo a dehydration process as located by endothermic peak in the range temperature 52.18–75.46 °C, depending upon the Zn:Ti molar ratio. Decomposition of the inorganic component such as Cl^- occurs in two steps, firstly in the temperature range 140.23–148.32 °C and secondly at 166.54 °C. The first decomposition step is observed for ZT13 and ZT11 powders and the second step is only detected for ZT11. The addition of HPC into the sols influences the process of organic decomposition which is shown by the exothermic peaks in the range 283.93–313.28 °C. This is consistent with the reported result for the composite TiO_2-HPC powder.[39] Dehydroxylation of Ti-OH into anatase-TiO_2 and rutile-TiO_2 can be ascribed by the small exothermic reactions located in the temperature range 400.65–472.17 °C. This is in good agreement with the crystallisation temperature of sol–gel derived TiO_2 powders reported previously.[40]

Furthermore, the peaks corresponding to crystallisation of zinc titanate ($ZnTiO_3$) are observed in the range 481.60–517.71. There is a small exothermic peak for ZT13 and ZT11, whereas it is a sharp peak for ZT31 powder. Therefore, it can be concluded that the crystallisation of zinc oxide (ZnO) also occurs in the above mentioned region for ZT31 powder. It means there is an overlap for the exothermic reactions concerning the formation of $ZnTiO_3$ and ZnO for ZT31 powder. These results are consistent with those obtained by XRD analysis. A broad exothermic peak localized around 850 °C is attributed to the crystallisation of titanium zinc oxide (Zn_2TiO_4).

The weight loss of $ZnTiO_3$ powders occurs at six stages. In the first stage (below 76 °C), the weight loss is a result of the evaporation of water. In the second stage, from 76 to 148 °C, the weight loss is ascribed to the further evaporation of water and decomposition of the inorganic component. Further decomposition of the inorganic compound takes place in the third stage, from 148 to 167 °C. Decomposition of HPC occurs in the fourth stage (in the range 284–313 °C). In the fifth stage, in the temperature range 442–472 °C, the weight loss is attributed to the

Table 5
Description of peak position and weight loss for the powders determined by SDT analysis.

Sample	ZT13		ZT11		ZT31	
Stages	Peak position (°C)	Weight loss (%)	Peak position (°C)	Weight loss (%)	Peak position (°C)	Weight loss (%)
Water evaporation	52.18	13.58	64.58	16.78	75.46	21.11
Further water evaporation and first step for decomposition of inorganic compound	148.32	17.47	140.23	21.28	–	13.19
Second step for decomposition of inorganic compound	–		166.54		–	
HPC decomposition	283.93	12.99	297.62	5.75	313.28	11.39
Crystallisation of anatase and rutile and further decomposition of organic compounds	442.82	8.37	400.65	12.47	472.17	18.25
Crystallisation of zinc titanate and further decomposition of organic compounds	511.64	4.16	481.60	23.10	517.71	16.90
Crystallisation of titanium zinc oxide	855.72	0	850	0	853.70	0

further decomposition of the organic compounds, arising from HPC, and formation of the anatase-TiO_2 and rutile-TiO_2 phases. In the last stage, in the region 482–518 °C, the weight loss is ascribed to the formation of the zinc titanate for all powders as well as cystallisation of zinc oxide for ZT31 powder. Since there is no weight loss after the last stage, the minimum sintering temperature to obtain organic- and inorganic-free powder can be determined at 570 °C for ZT13 powder, 530 °C for ZT11

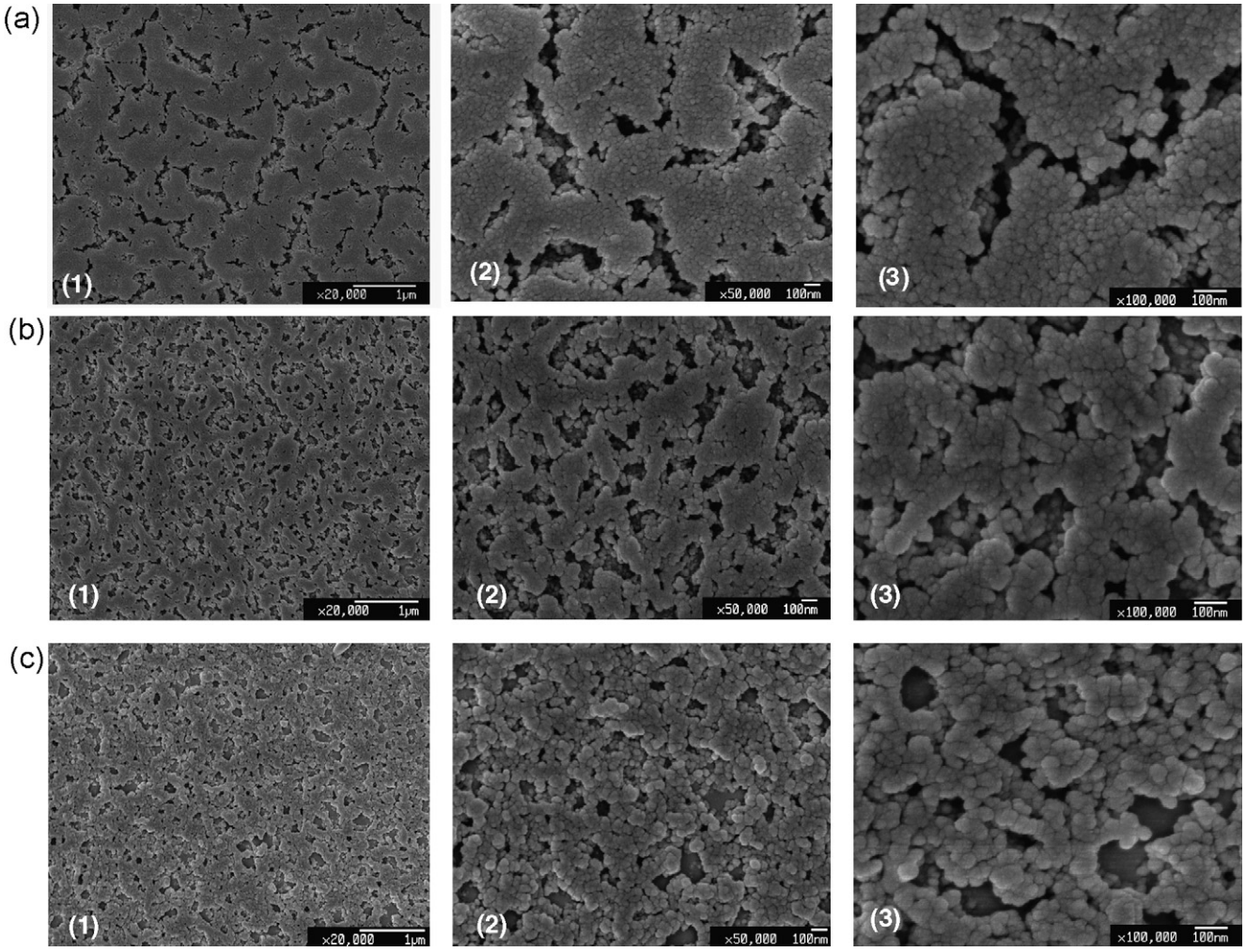

Fig. 11. Surface morphology of the films sintered at 600 °C for 1 h as a function of component composition change: (a) ZT13, (b) ZT11 and (c) ZT31.

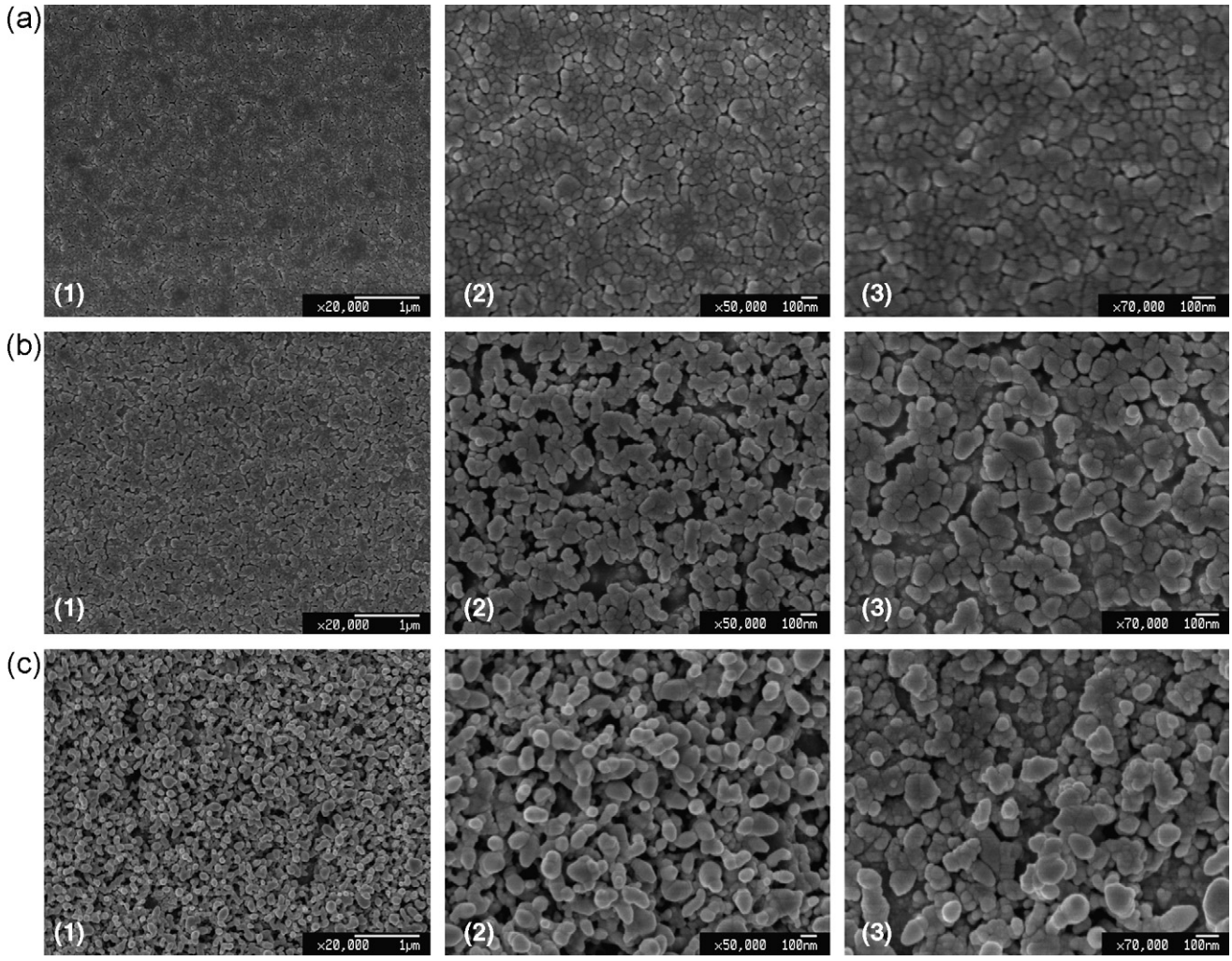

Fig. 12. Surface morphology of the films sintered at 800 °C for 1 h as a function of component composition change: (a) ZT13, (b) ZT11 and (c) ZT31.

and 520 °C for ZT31 powders. Consequently, the ultimate sintering temperature for entire elimination of organic and inorganic components reduced with increasing Zn:Ti molar ratio.

3.5. Microstructure

Figs. 11 and 12 show surface micrographs of sol–gel prepared thin films sintered at 600 and 800 °C for 1 h, respectively.

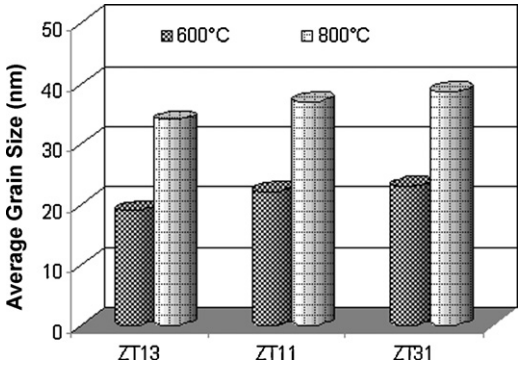

Fig. 13. Effect of Zn:Ti molar ratio on average grain size of the thin films sintered at 600 and 800 °C for 1 h.

It can be observed that all deposited films had crystalline structure, which is in good agreement with the XRD results. In all cases, relatively dense, homogeneous, nano-grains and crack-free films were obtained. This could be supported by the fact that employment of water with low evaporation rate, as dispersant media, has kept films crack free. In addition, the interstices between the particles caused by HPC are noticeable resulting in a porous structure with irregular pore shape. The porosity percentage of 600 °C films decreased with increasing Zn:Ti molar ratio, while the reverse trend was obtained for the films annealed at 800 °C. Owing to the fact that the equal HCl concentration was used for preparation of TiO_2 sol, the HCl:(Zn + Ti) molar ratio reduced with increasing Zn:Ti molar ratio. The lower HCl:(Zn + Ti) molar ratio, the lower surface charge around the particles, resulting in reducing the electrostatic repulsion and finally the porosity of 600 °C sintered films. For 800 °C sintered films, this can be explained by the fact that the decomposition of zinc chloride is an exothermic reaction (as confirmed by SDT analysis in Section 3.4) and the released fumes avoid sintering the particles and reducing the porosity. Moreover, the porosity of the films is reduced with increasing annealing temperature due to the sintering of particles at high temperature. Therefore,

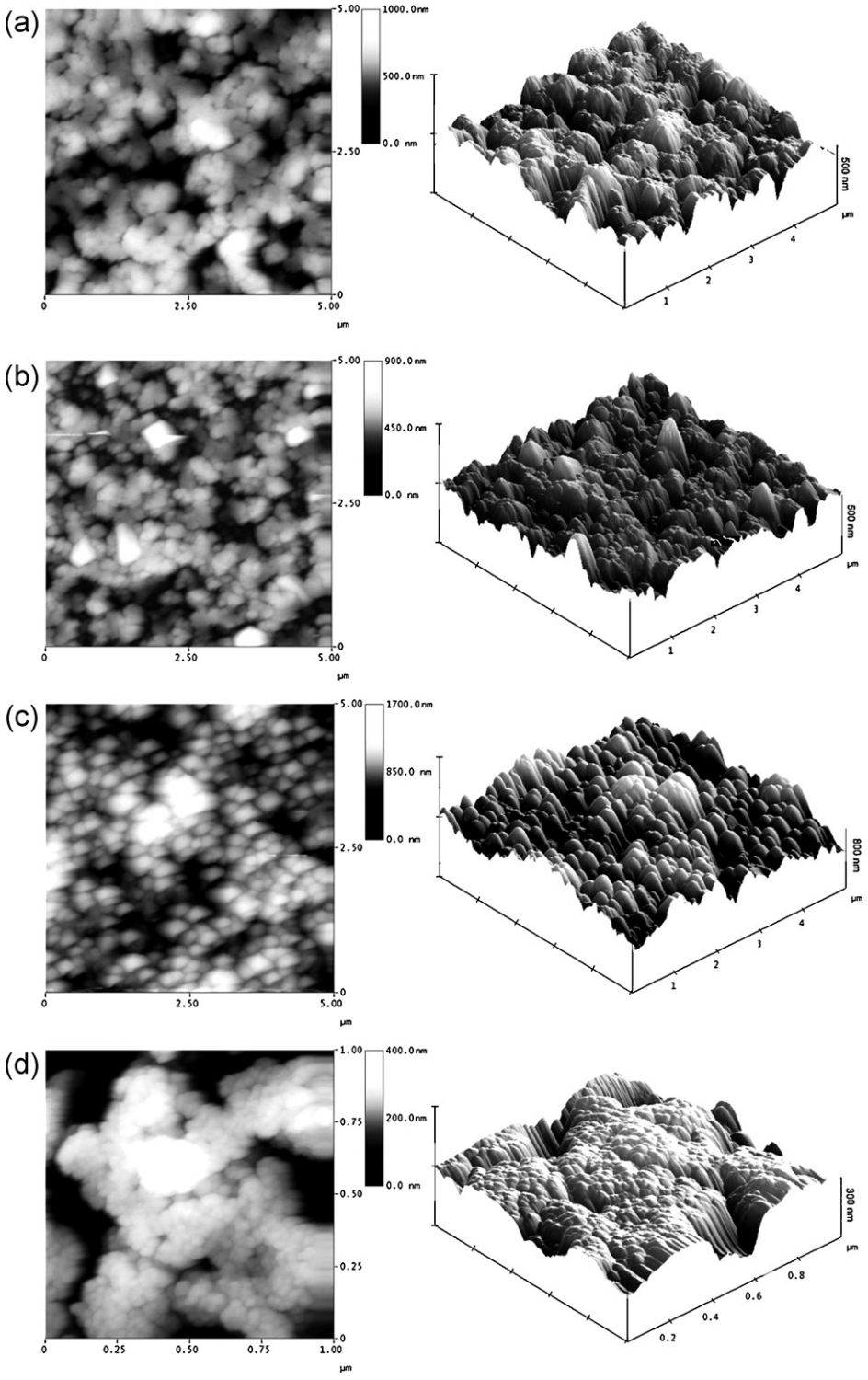

Fig. 14. Atomic force micrographs of $ZnTiO_3$ films sintered at 600 °C for 1 h: (a) ZT13 (5 μm × 5 μm), (b) ZT11 (5 μm × 5 μm), (c) ZT31 (5 μm × 5 μm) and (d) ZT13 (1 μm × 1 μm).

it is possible to control the densification process (i.e., porosity reduction) of $ZnTiO_3$ films by two parameters of Zn:Ti molar ratio and heat treatment temperature. It is interesting to note that the homogeneity in grain size distribution for titanium dominant films (i.e., ZT13) is better than that of for the rest of the films, especially at high temperature. This can be related to the presence of ZnO in zinc dominant films (i.e., ZT31). As shown in Fig. 4, ZnO had the highest average crystallite size amongst anatase-TiO_2, rutile-TiO_2 and $ZnTiO_3$. Therefore the bigger grains, in Fig. 12-c, are labeled as ZnO.

Based on the FE-SEM images, the dependence of the average grain size of the deposited thin films on the Zn:Ti molar ratio is shown in Fig. 13. The average grain size of the films sintered at 600 °C is around 19 nm for ZT13, 22 nm for ZT11 and 23 nm for ZT31. Heat treatment at 800 °C induced a gradual increase occurred, being 34, 37 and 39 nm for ZT13, ZT11 and ZT31 films, respectively. Thus, ZT13 film (i.e., the titanium dominant film) had the smallest grain size amongst the sintered films. These results are consistent with those obtained by XRD analysis, given that ZT13 powder possessed the smallest crystallite size. It should be noted that, the deposited thin films have good thermal stability against heat treatment due to a slight increase in grain size at high temperature.

3.5.1. AFM analysis

Fig. 14 illustrates 2D and 3D topographies of the thin films sintered at 600 °C for 1 h. As can be observed in 2D images, all deposited films show that they are homogeneous, rough and uniform with nano-sized grains. Based on 3D images, it can be concluded that ZT13 and ZT11 films have a hill-valley like morphology made up of small grains, whereas ZT31 film show a columnar like morphology. Fig. 14-d confirms that the deposited zinc titanate film, by a particulate sol–gel process, is a nanostructured and porous thin film.

4. Conclusions

Low temperature sol–gel derived zinc titanate ($ZnTiO_3$) thin films and powders with nanocrystalline structure have been successfully prepared. Titanium isopropoxide and zinc chloride were used as titanium and zinc precursors, whereas HPC was used as a PFA. It was found that the prepared sols were stable over 5 months, since the constant zeta potentials were measured during this period, being in the range 38.2–47.1 mV at pH 1–2. It was found that the phase composition and crystallite size of the samples depends on Zn:Ti molar ratio and sintering temperature. Based on XRD analysis, the maximum $ZnTiO_3$ percentage of 94% was achieved for ZT31 powder at the low sintering temperature of 500 °C and the short sintering time of 1 h. Moreover, TiO_2 content was decreased with increasing Zn:Ti molar ratio and decreasing the sintering temperature. It was found that the decomposition temperature of $ZnTiO_3$ decreased down to 600 °C with increasing Zn:Ti molar ratio ≥75:25. The average crystallite size of $ZnTiO_3$ phase decreases with decreasing Zn:Ti molar ratio at all sintering temperatures. SDT analysis showed that the minimum sintering temperature to obtain organic- and inorganic-free powder reduced with increasing Zn:Ti molar ratio around 570 °C for 1 h. FE-SEM images showed that in all cases relatively dense, homogeneous, nano-grains and crack-free films were obtained. The porosity percentage of 600 °C films decreased with increasing Zn:Ti molar ratio, while the reverse trend was obtained for the films sintered at 800 °C. AFM analysis confirmed that the deposited zinc titanate film had nanocrystalline and porous structure with roughness mean square (rms) in the range 45–65 nm.

Acknowledgement

The authors wish to acknowledge Mr. David Nicol for his help with TEM analysis.

References

1. Yamamoto, O., Takeda, Y., Kanno, R. and Noda, M., Perovskite-type oxides as oxygen electrodes for high temperature oxide fuel cells. *Solid State Ionics*, 1987, **22**, 241–246.
2. Shimizu, Y., Uemura, K., Miura, N. and Yamazoe, N., Gas-diffusion electrodes for oxygen reduction loaded with large surface area $La_{1-x}Ca_xMO_3$ (M = Co,Mn). *Chem. Lett.*, 1988, **12**, 1979–1982.
3. Obayashi, H., Sakurai, Y. and Gejo, T., Perovskite-type oxides as ethanol sensors. *J. Solid State Chem.*, 1976, **17**, 299–303.
4. Takehira, K., Shishido, T. and Kondo, M., Partial oxidation of CH_4 over $Ni/SrTiO_3$ catalysts prepared by a solid-phase crystallization method. *J. Catal.*, 2002, **207**, 307–316.
5. McCord, A.T. and Saunder, H.F., U.S. Patent 2739019, *Ceram. Abstr.*, 1945, **24**, 155.
6. Ozdemir, S. and Bardakci, T., Hydrogen sulfide removal from coal gas by zinc titanate sorbent. *Sep. Purif. Technol.*, 1999, **16**, 225–234.
7. Kim, H. T., Nahm, S. and Byun, J. D., Low-fired $(Zn, Mg)TiO_3$ microwave dielectrics. *J. Am. Ceram. Soc.*, 1999, **82**, 3476–3480.
8. Wakino, K., Nischicawa, T., Ishikawa, Y. and Tamura, H., Dielectric resonator materials and their applications for mobile communication systems. *Br. Ceram. Trans. J.*, 1990, **89**, 39–43.
9. Sreemoolanadhan, H., Sebastian, M. T. and Mohanan, P., High permittivity and low loss ceramics in the $BaO\text{-}SrO\text{-}Nb_2O_5$ system. *Mater. Res. Bull.*, 1995, **30**, 653–658.
10. Kim, H. T., Byun, J. D. and Kim, Y., Microstructure and microwave dielectric properties of modified zinc titanates. *Mater. Res. Bull.*, 1998, **33**, 963–973.
11. Dulin, F. H. and Rase, D. E., Phase equilibria in the system $ZnO–TiO_2$. *J. Am. Ceram. Soc.*, 1960, **43**, 125–131.
12. Bartram, S. F. and Slepetys, R. A., Compound formation and crystal structure in the system $ZnO–TiO_2$. *J. Am. Ceram. Soc.*, 1961, **44**, 493–499.
13. Yamaguchi, O., Morimi, M., Kawabata, H. and Shimizu, K., Formation and transformation of $ZnTiO_3$. *J. Am. Ceram. Soc.*, 1987, **70**, C97–C98.
14. Luo, J., Xing, X., Yu, R., Xing, O., Zhang, D. and Chen, X., Synthesis and characterization of $(Zn,Co)TiO_3$ by modified low temperature preparing route. *J. Alloys Compd.*, 2005, **402**, 263–268.
15. Chang, Y. S., Chang, Y. H., Chen, I. G., Chen, G. J., Chai, Y. L., Fang, T. H. and Wu, S., Synthesis, formation and characterization of $ZnTiO_3$ ceramics. *Ceram. Int.*, 2004, **30**, 2183–2189.
16. Jun, H. K., Lee, T. J., Ryu, S. O. and Kim, J. C., A study of Zn-Ti-based. H_2S removal sorbents promoted with cobalt oxides. *Ind. Eng. Chem. Res.*, 2001, **40**, 3547–3556.
17. Alonso, L., Palacios, J. M. and Moliner, R., The performance of some ZnO-based regenerable sorbents in hot coal gas desulfurization long-term tests using graphite as a pore-modifier additive. *Energy Fuel*, 2001, **15**, 1396–1402.
18. Pineda, M., Fierro, J. L. G., Palacios, J. M., Cilleruelo, C., Garcia, E. and Ibarra, J. V., Characterization of zinc oxide and zinc ferrite doped with Ti or Cu as sorbents for hot gas desulphurization. *Appl. Surf. Sci.*, 1997, **119**, 1–10.
19. Jothimurugesan, K. and Gangwal, S. K., Regeneration of zinc titanate H_2S sorbents. *Ind. Eng. Chem. Res.*, 1998, **37**, 1929–1933.
20. Lew, S., Sarofim, A. F. and Flytzani-Stephanopoulos, M., The reduction of zinc titanate and zinc oxide-solids. *Chem. Eng. Sci.*, 1992, **47**, 1421–1431.
21. Phani, A. R. and Santucci, S., Effect of annealing temperature in the formation of rhombohedral phase in cubic-zinc titanium oxide thin films by sol-gel technique. *J. Mater. Sci. Lett.*, 2001, **20**, 573–575.
22. Chang, Y. S., Chang, Y. H., Chen, I. G., Chen, G. J. and Chai, Y. L., Synthesis and characterization of zinc titanate nano-crystal powders by sol–gel technique. *J. Cryst. Growth*, 2002, **243**, 319–326.

23. Chang, Y. S., Chang, Y. H., Chen, I. G., Chen, G. J., Chai, Y. L., Fang, T. H. and Wu, S., Formation and characterization of $ZnTiO_3$ ceramics. *Ceram. Int.*, 2004, **30**, 2183–2189.
24. Zhao, L., Liu, F., Wang, X., Zhang, Z. and Yan, J., Preparation and characterizations of $ZnTiO_3$ powders by Sol–Gel process. *J. Sol-Gel Sci. Technol.*, 2005, **33**, 103–106.
25. Hou, L., Hou, Y. D., Zhu, M. K., Tang, J., Liu, J. B., Wang, H. and Yan, H., Formation and transformation of $ZnTiO_3$ prepared by sol–gel process. *Mater. Lett.*, 2005, **59**, 197–200.
26. Phani, A. R., Passacantando, M. and Santucci, S., Synthesis of nanocrystalline $ZnTiO_3$ perovskite thin films by sol–gel process assisted by microwave irradiation. *J. Phys. Chem. Solids*, 2007, **68**, 317–323.
27. Chai, Y. L., Chang, Y. S., Chen, G. J. and Hsiao, Y. J., The effects of heat-treatment on the structure evolution and crystallinity of $ZnTiO_3$ nano-crystals prepared by Pechini process. *Mater. Res. Bull.*, 2008, **43**, 1066–1073.
28. Manik, S. K. and Pradhan, S. K., Preparation of nanocrystalline microwave dielectric Zn_2TiO_4 and $ZnTiO_3$ mixture and X-ray microstructure characterization by Rietveld method. *Physica E*, 2006, **33**, 69–76.
29. Mohammadi, M. R., Cordero-Cabrera, M. C., Ghorbani, M. and Fray, D. J., Synthesis of high surface area nanocrystalline anatase-TiO_2 powders derived from particulate sol-gel route by tailoring processing parameters. *J. Sol-Gel Sci. Technol.*, 2006, **40**, 15–23.
30. Mohammadi, M. R., Cordero-Cabrera, M. C., Fray, D. J. and Ghorbani, M., Preparation of high surface area titania (TiO_2) films and powders using particulate sol–gel route aided by polymeric fugitive agents. *Sens. Actuators B*, 2006, **120**, 86–95.
31. Cullity, B. D., *Elements of X-ray Diffraction*. Addison-Wesley, London, 1978, p. 99.
32. Jarcho, M., Bolen, C. H. and Doremus, R. H., Hydroxyaptite synthesis and characterization in dense polycrystalline form. *J. Mater. Sci.*, 1976, **11**, 2027–2035.
33. Mohammadi, M. R., Fray, D. J. and Mohammadi, A., Sol–gel nanostructured titanium dioxide: controlling the crystal structure, crystallite size, phase transformation, packing and ordering. *Microporous Mesoporous Mater.*, 2008, **112**, 392–402.
34. Malvern Instruments, *DST Customer Training Manual for Zeta Potential*, 2003, Chapter 6.
35. Ivanova, T., Harizanova, A. and Surtchev, M., Formation and investigation of sol–gel TiO_2-V_2O_5 system. *Mater. Lett.*, 2002, **55**, 327–333.
36. Socrates, G., *Infrared Characteristic Group Frequencies: Tables and Charts*. John Wiley & Sons, England, 1994, p. 6, 62 and 237.
37. Last, J. T., Infrared-absorption studies on barium titanate and related materials. *Phys. Rev.*, 1957, **105**, 1740–1750.
38. Liu, X. C., Zhao, L. L., Gao, F., Yan, X. B. and Tian, C. S., Phase transition and grain growth kinetics of V_2O_5 and B_2O_3 doped zinc titanate ceramics. *J. Inorg. Mater.*, 2006, **21**, 885–892.
39. Mohammadi, M. R., Ghorbani, M., Cordero-cabrera, M. C. and Fray, D. J., Preparation and characterisation of nanostructural TiO_2-Ga_2O_3 binary oxides with high surface area derived form particulate sol–gel route. *J. Mater. Sci.*, 2007, **42**, 4976–4986.
40. Mohammadi, M. R., Fray, D. J., Sadrnezhaad, S. K. and Mohammadi, A., A simple particulate sol–gel route to synthesize nanostructural TiO_2-Ta_2O_5 binary oxides and their characteristics. *Mater. Sci. Eng. B*, 2007, **142**, 16–27.